

NANO EXPRESS

Open Access



Photocatalytic Activities Enhanced by Au-Plasmonic Nanoparticles on TiO₂ Nanotube Photoelectrode Coated with MoO₃

Chia-Jui Li¹, Chuan-Ming Tseng^{2*}, Sz-Nian Lai¹, Chin-Ru Yang¹ and Wei-Hsuan Hung^{1*} 

Abstract

Although TiO₂ was formerly a common material for photocatalysis reactions, its wide band gap (3.2 eV) results in absorbing only ultraviolet light, which accounts for merely 4% of total sunlight. Modifying TiO₂ has become a focus of photocatalysis reaction research, and combining two metal oxide semiconductors is the most common method in the photocatalytic enhancement process. When MoO₃ and TiO₂ come into contact to form a heterogeneous interface, the photogenerated holes excited from the valence band of MoO₃ should be transferred to the valence band of TiO₂ to effectively reduce the charge recombination of photogenerated electron–hole pairs. This can efficiently separate the pairs and promote photocatalysis efficiency. In addition, photocurrent enhancement is attributed to the strong near-field and light-scattering effects from plasmonic Ag nanoparticles. In this work, we fabricated MoO₃-coated TiO₂ nanotube heterostructures with a 3D hierarchical configuration through two-step anodic oxidation and a facile hydrothermal method. This 3D hierarchical structure consists of a TiO₂ nanotube core and a MoO₃ shell (referred to as TNTs@MoO₃), as characterized by field emission scanning electron microscopy and X-ray photoelectron spectroscopy.

Keywords: Metal oxide, Core–shell structure, Plasmonic nanoparticles, Photocatalysis reaction

Background

Rapid technological development has been accompanied by an increased demand for energy. Consequently, research into alternative energy sources has become popular over the past decade, with many scientists focused on renewable energy sources with low carbon emissions and minimal environmental impact. These include solar energy [1, 2], geothermal heat [3, 4], tides [5], and various forms of biomass [6, 7]. Photocatalytic water splitting, as the most direct method for achieving the goal of clean and renewable energy [8], is also the most investigated method of directly converting solar energy into chemical energy. Some common means of promoting energy conversion efficiency include increasing the reaction area, catalyst deposition, and compositing with secondary materials; for example, synthesizing specific microstructures [9–11],

depositing Pt as a catalyst [12, 13], and combining two different metal oxides [14–16].

TiO₂ nanotube (TNT) arrays have received considerable attention for their large surface area, robust photocatalytic activity, and vectorial charge transfer properties [17–19]. However, the practical application of TiO₂ is restricted by its wide band gap (3.2 eV). This results in absorbing only UV light, which accounts for 4% of total sunlight, greatly limiting its photocatalytic activity in the visible light region. In addition, the high recombination rate of TiO₂ lowers the efficiency of photocatalytic activity. To solve these problems, many studies have focused on extending the absorption edge of TiO₂ into the visible light region, including doping with nitrogen or other nonmetals [20, 21], surface modification with noble metals [22, 23], and coupling with narrow-band-gap semiconductors [14–16].

Molybdenum trioxide (MoO₃) is a p-type metal oxide semiconductor with a high work function and excellent hole conductivity; therefore, it is widely used in organic solar cells and organic light-emitting diodes [24, 25].

* Correspondence: cmtseng@mail.mcut.edu.tw; whung@fcu.edu.tw

²Department of Materials Engineering, Ming Chi University of Technology, New Taipei City, Taiwan

¹Department of Material Science and Engineering, Feng Chia University, Taichung, Taiwan

MoO₃ has a band gap of approximately 2.8 eV, with 20–30% ionic character and the capacity to absorb both UV and visible light [26]. The valence and conduction band positions of MoO₃ are both lower than those of TiO₂. Hence, a heterojunction between TiO₂ and MoO₃ might enhance photocatalytic activity by decreasing the charge recombination and promoting the charge transfer process [27]. Under visible light irradiation, the holes excited from the valence band of MoO₃ should be transferred to the valence band of TiO₂, to reduce the charge recombination of photogenerated electron–hole pairs.

Plasmonic photocatalysis has recently facilitated the rapid enhancement of photocatalytic efficiency under visible light irradiation [28, 29]. A surface plasmon is a surface electromagnetic wave on the metal–dielectric interface, widely used in optical, chemical, and biological sensing for the high sensitivity of its resonant waves. The surface plasmon resonance effect is confined to the metal surface to form a highly enhanced electric field [30]. When the particular resonance frequency of plasmonic metal nanoparticles matches that of the incident photon, strong electric field forms near the surface of the metal. Furthermore, tunable interactions between incident visible light and excited plasmonic nanoparticles are achieved by controlling their sizes and shapes, as well as the dielectric constant of the surrounding environment [31–33].

In the present work, we first synthesized MoS₂ coating on the surface of TNTs through a hydrothermal method. MoS₂ was then oxidized to MoO₃ through a simple annealing process (Scheme 1). This process enabled high coverage of MoO₃ nanoscale particles with a highly ordered structure. To further enhance the photocatalytic water-splitting performance, we introduced a surface plasmon resonance (SPR) effect.

Methods

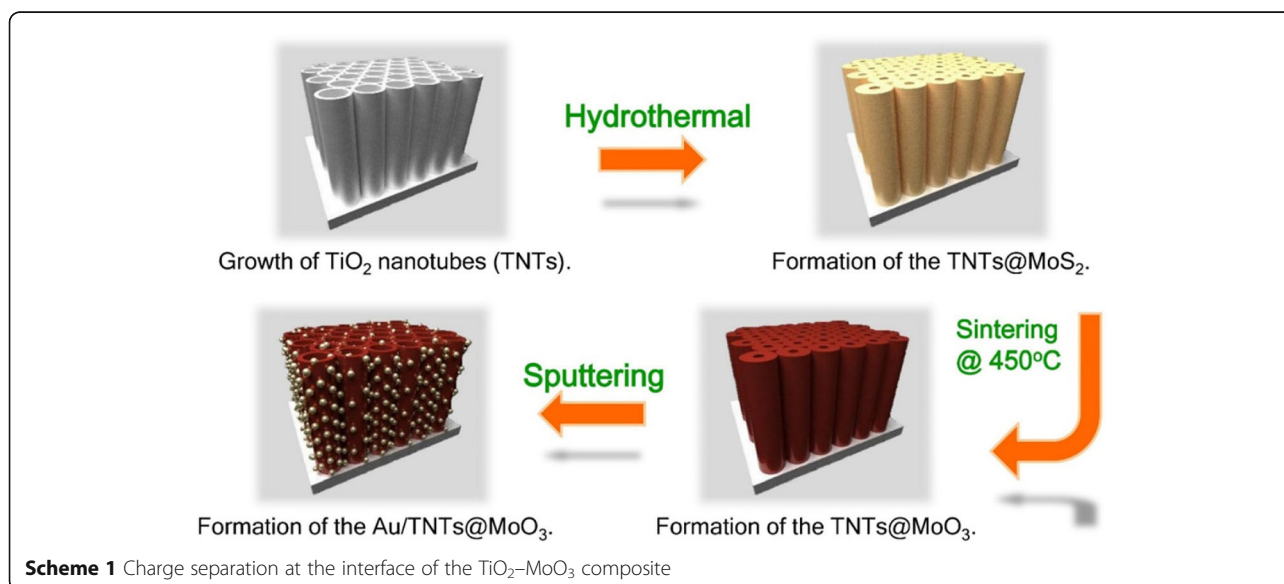
Fabrication of the TiO₂ Nanotubes

The TNTs were fabricated by a two-step anodic oxidation method. Prior to the anodic oxidation process, the titanium foil was cut to size and placed in acetone, then ethanol, then deionized (DI) water, and then subjected to ultrasonic vibration for 5 min. Anodic oxidation was carried out using a conventional two-electrode system with the Ti foil as an anode and a carbon rod as a cathode. All electrolytes consisted of 0.3 wt% ammonium fluoride (NH₄F) in ethylene glycol (C₂H₆O₂, EG) solution with 5 vol% water. All processes were carried out at room temperature.

In the first step of anodic oxidation, the Ti foil was anodized at 60 V for 30 min; the as-grown nanotubes were subsequently removed in 1 M HCl by ultrasonic vibration. The same Ti foil then underwent a second anodic oxidation process at 60 V for 30 min. After both steps were completed, the prepared TNTs were washed with ethanol and DI water. The TNTs were annealed in air at 450 °C for 4 h at a heating rate of 2 °C/min to form the anatase TNTs.

Synthesis of TNTs@MoO₃ Core–Shell Structure

The TNTs@MoO₃ core–shell structure was synthesized with a hydrothermal method and a simple annealing process. MoS₂ nanosheets were synthesized by the following procedures: 0.12 g of sodium molybdate (Na₂MoO₄·2H₂O) and 0.24 g of thioacetamide (TAA) were dissolved in 80 mL of DI water under vigorous stirring for 15 min. Subsequently, the transparent solution and as-grown TNTs were transferred into a 100-mL Teflon-lined stainless steel autoclave, which was sealed and heated to 200 °C at a heating rate of 3 °C/min and



held for 24 h. After the autoclave was cooled to room temperature, the prepared TNTs@MoS₂ were washed with DI water. The TNTs@MoS₂ were annealed in air at 450 °C for 4 h with a heating rate of 2 °C/min to form the TNTs@MoO₃ core-shell structure.

Deposition of Au Nanoparticles

The plasmonic cocatalyst photoelectrodes (Au/TNTs@MoO₃) were fabricated with the prepared TNTs@MoO₃ cocatalytic core-shell structure through the hydrothermal method, followed by the standard sputtering deposition of Au nanoparticles.

Characteristic Analysis and Photocurrent Measurements

The microstructures and morphologies of the samples were examined using field emission scanning electron microscopy (FE-SEM) and energy-dispersive X-ray spectroscopy (EDS). To confirm the bonding energy of the developed TiO₂, MoS₂, and MoO₃ photoelectrodes, X-ray photoelectron spectroscopy (XPS) was employed. Finally, the photocatalytic reaction was measured in 1 M NaOH solution by operating three terminal potentiostats at room temperature under 532-nm laser irradiation with a 1-mm diameter spot size.

Results and Discussion

Figure 1 shows the SEM images and EDS mapping of the prepared samples. Figure 1a–c shows the SEM images of the TNTs, TNTs@MoS₂, and TNTs@MoO₃. The SEM image of TNTs obtained by two-step anodic

oxidation of Ti foil in 0.3 wt% NH₄F contained in ethylene glycol solution (Fig. 1a) exhibited uniform pore size (100–120 nm). After the core-shell structure was formed with MoS₂ covered through the hydrothermal method, the porous structure of TNTs was not blocked to reduce the active reaction sites (Fig. 1b). Subsequently, the TNTs@MoO₃ core-shell structure was formed by a simple annealing process in the tube furnace (Fig. 1c). Figure 1d shows the SEM image and EDS mapping of Au/TNTs@MoO₃, providing clear information about the Ti, O, Mo, and Au. The uniform deposition of the island-like Au nanoparticles, observable on top of the TNTs@MoO₃, facilitated the generation of the SPR effect.

XPS was used to investigate the chemical states of the TNTs@MoO₃ after conversion from TNTs@MoS₂ through a simple annealing process (Fig. 2). Three characteristic peaks of Ti and O can be observed in Fig. 2a, b. The binding energies at the Ti2p₁, Ti2p₃, and O1s peaks are 464.6, 458.9, and 530.4 eV, respectively. In Fig. 2c, a Mo3d₃ peak at 231.6 eV and Mo3d₅ peak at 228.9 eV can be identified, indicating the chemical composition of MoS₂ in the TNTs@MoS₂. In addition, a weak peak appearing at approximately 226 eV is the signal peak of S2s. The Mo3d₃ and Mo3d₅ peaks in Fig. 2d with binding energies of 235.6 and 232.6 eV are ascribed to Mo⁶⁺ in MoO₃. Therefore, the XPS investigations confirm that the red shift of the spectrum reflects the conversion of the Mo element valence from tetravalent to hexavalent.

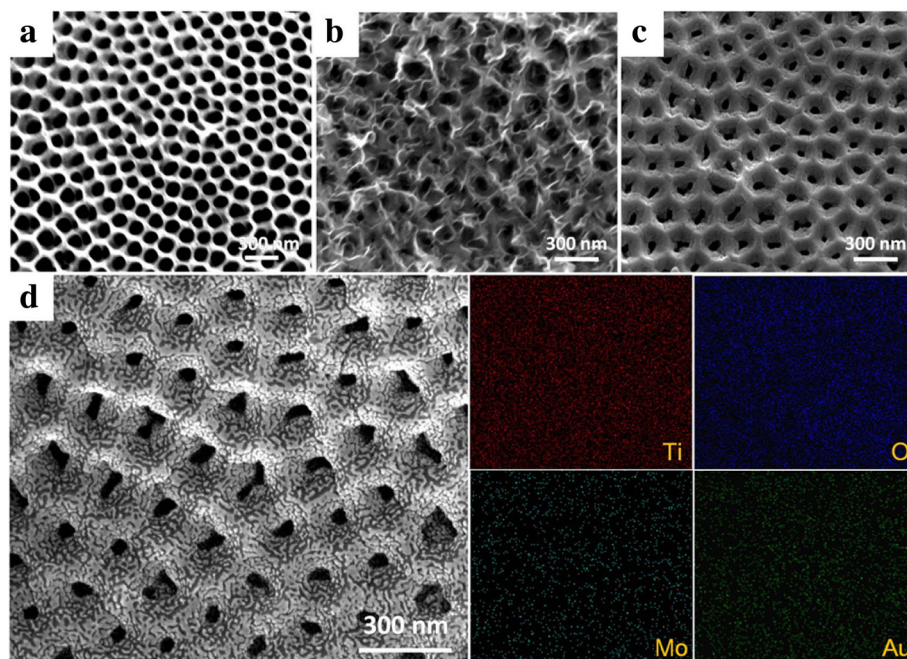
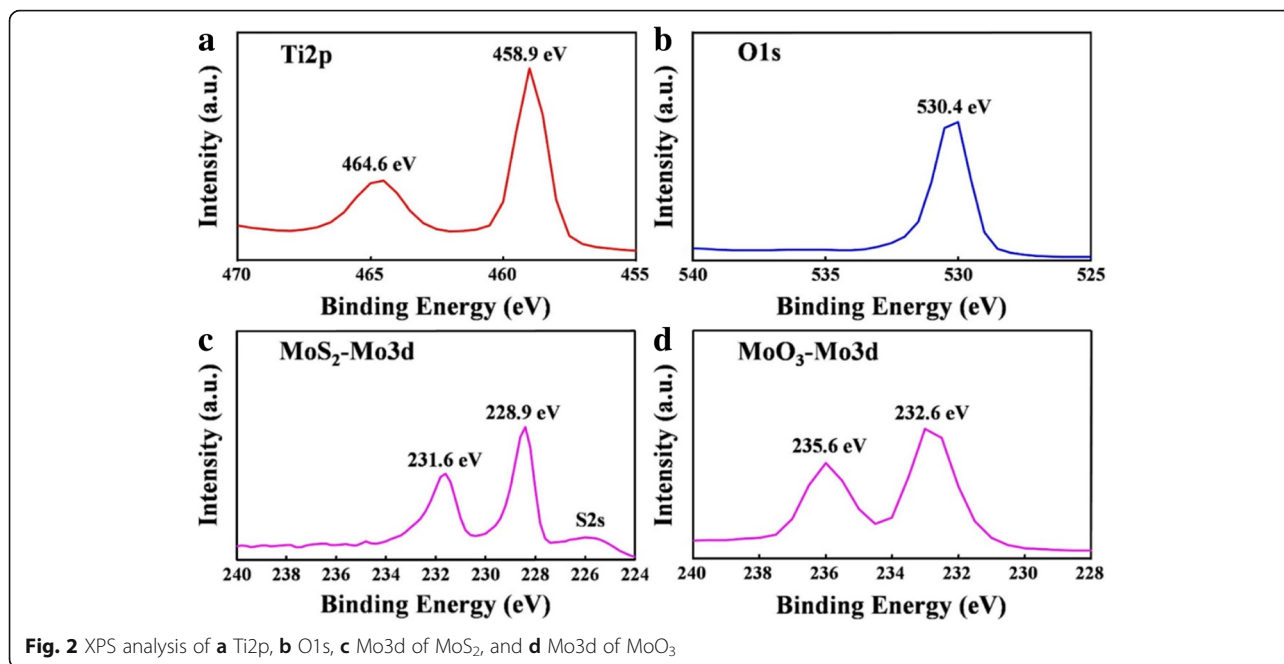
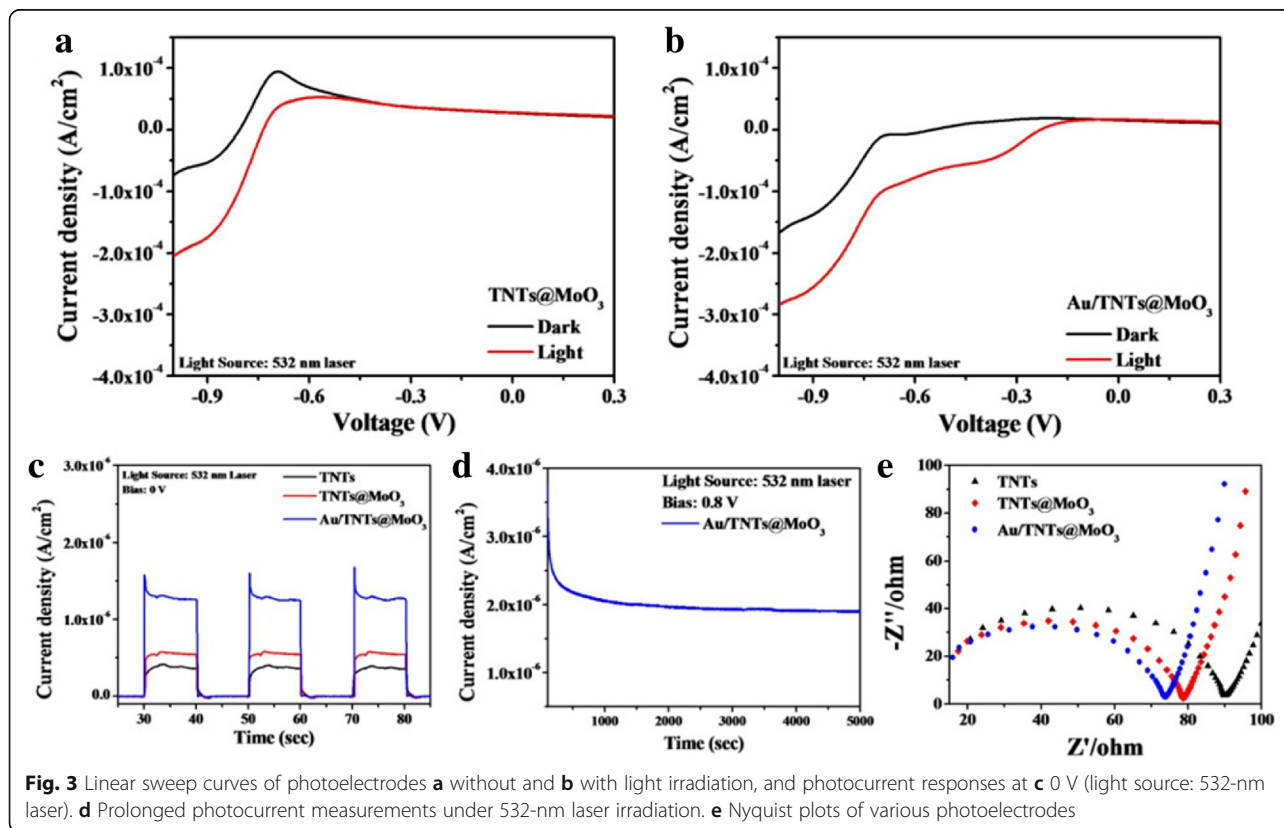


Fig. 1 SEM images of **a** TNTs, **b** TNTs@MoS₂, **c** TNTs@MoO₃, and **d** Au/TNTs@MoO₃ (left), as well as EDS mapping (right)



The photocatalytic water-splitting performance of the prepared photoelectrodes was measured under 532-nm laser irradiation. Figure 3a, b shows the photocurrent response (*I*-*V* curves) of TNTs@MoO₃ and Au/TNTs@MoO₃. According to the results, TiO₂@MoO₃

exhibits a higher photocurrent because of the enhanced charge separation rate at the TiO₂@MoO₃ heterogeneous interface (shown in Fig. 3a). Furthermore, with the integration of Au nanoparticles, Au/TNTs@MoO₃ presented a photocurrent response approximately 1.5 times higher than



TNTs@MoO₃ at the bias voltage of -1 V. Figure 3c shows the I-T curves of the TNTs, TNTs@MoO₃, and Au/TNTs@MoO₃ at the bias voltage of 0 V. As shown in Fig. 3c, the photocurrent response was higher again in the Au/TNTs@MoO₃ structure compared to the TNTs@MoO₃ photoelectrode without the application of bias voltage. The photocurrent response of Au/TNTs@MoO₃ could be enhanced through the simple SPR effect.

To further investigate the photocatalytic activity of the prepared photoelectrodes, we also examined the extended photocurrent responses and electrochemical impedance spectroscopy to understand the photocurrent stability and the charge transfer at the photoelectrode-electrolyte interfaces (Fig. 3d, e). The extended stability of the photoelectrode with the optimal performance, Au/TNTs@MoO₃, was examined under 532-nm laser irradiation for approximately 1.5 h (Fig. 3d). At the applied voltage of 0.8 V, the photocurrent remained at 57% of its initial value. Figure 3e shows the Nyquist plots of all three tested photoelectrodes under 532-nm laser irradiation recorded at a DC potential of 1.23 V versus RHE and an AC potential frequency range of 10⁶-1 Hz with an amplitude of 1 V under 532-nm laser irradiation. According to the results, smaller semicircle diameters can be observed in the Au/TNTs@MoO₃ sample, indicating a lower transport impedance for charge carriers. The formation of a heterogeneous interface between TiO₂ and MoO₃ is confirmed to facilitate charge transfer and enhance photocatalytic activity through the excellent carrier conduction properties of the Au nanoparticles.

Conclusions

Supporting information

In the supporting information (Additional file 1) we performed the Raman spectra analysis of MoS₂ layer, the related thickness and average pore size of SEM images of TNTs, and the enhancement mechanism of the system.

In this study, we successfully fabricated a TNTs@MoS₂ core-shell heterostructure by a two-step anodic oxidation process and a facile hydrothermal method to form a TNTs@MoO₃ core-shell structure through a simple annealing process. According to the results, a MoO₃ coating on a photoelectrode can enhance its utilization of photons in the visible region. Moreover, with the integration of plasmonic Au nanoparticles, a significant improvement in the water-splitting photocurrent was observed compared to pure TiO₂ nanotubes under visible light irradiation. The energy band engineering of the TNTs@MoO₃ heterostructure favors charge transfer and suppresses photogenerated electron-hole pair recombination between MoO₃ and TiO₂, leading to enhanced photocatalytic activity.

Additional file

Additional file 1: Supporting information. (DOCX 1074 kb)

Funding

The authors acknowledge financial support from the Ministry of Science and Technology Foundation (MOST 105-2221-E-035-015-). The authors appreciate the Precision Instrument Support Center of Feng Chia University for providing the facilities for production and measurement.

Authors' Contributions

CJL carried out the experiments and drafted the manuscript. SNL participated in the design of the study and performed the analysis. CRY participated in the measurements. CMT and WHH supervised the overall study and polished the manuscript. All authors read and approved the final manuscript.

Competing Interests

The authors declare that they have no competing interests.

Publisher's Note

Springer Nature remains neutral with regard to jurisdictional claims in published maps and institutional affiliations.

Received: 20 June 2017 Accepted: 26 September 2017

Published online: 06 October 2017

References

1. Yang Y, Yang WZ, Tang WD, Sun CD (2013) High-temperature solar cell for concentrated solar-power hybrid systems. *Appl Phys Lett* 103:8
2. Zhang Y, Wang H, Liu Z, Zou B, Duan CY, Yang T, Zhang XJ, Zheng CJ, Zhang XH (2013) Optical absorption and photoelectrochemical performance enhancement in Si tube array for solar energy harvesting application. *Appl Phys Lett* 102:16
3. Bojadgieva K, Benderev A, Berova-Andonova A, Tsanov T (2013) Aspects of current geothermal application in Bulgaria. *J Renew Sustain Ener* 5:4
4. Self SJ, Reddy BV, Rosen MA (2013) Geothermal heat pump systems: status review and comparison with other heating options. *Appl Energy* 101:341-348
5. Wang L, Li CN (2011) Dynamic stability analysis of a tidal power generation system connected to an onshore distribution system. *Ieee T Energy Convers* 26(4):1191-1197
6. Laihanen M, Karhunen A, Ranta T (2013) Possibilities and challenges in regional forest biomass utilization. *J Renew Sustain Ener* 5:3
7. Lei TZ, Wang ZW, Li ZF, Xu JF, He XF, Zhu JL (2013) A biomass briquetting fuel machine and its large-scale operation system. *J Renew Sustain Ener* 5:1
8. Hung WH, Chien TM, Tseng CM (2014) Enhanced photocatalytic water splitting by plasmonic TiO₂-Fe₂O₃ cocatalyst under visible light irradiation. *J Phys Chem C* 118(24):12676-12681
9. Chae SY, Sudhagar P, Fujishima A, Hwang YJ, Joo OS (2015) Improved photoelectrochemical water oxidation kinetics using a TiO₂ nanorod array photoanode decorated with graphene oxide in a neutral pH solution. *Phys Chem Chem Phys* 17(12):7714-7719
10. Yantara N, Pham TTT, Boix PP, Mathews N (2015) Modulating light propagation in ZnO-Cu₂O-inverse opal solar cells for enhanced photocurrents. *Phys Chem Chem Phys* 17(33):21694-21701
11. Liu XY, Huang JA, Yang B, Zhang XJ, Zhu YY (2015) Highly reproducible SERS substrate based on polarization-free Ag nanoparticles decorated SiO₂/Si core-shell nanowires array. *AIP Adv* 5:5
12. Wang CC, Hsueh YC, Su CY, Kei CC, Perng TP (2015) Deposition of uniform Pt nanoparticles with controllable size on TiO₂-based nanowires by atomic layer deposition and their photocatalytic properties. *Nanotechnology* 26:25
13. Haldorai Y, Rengaraj A, Lee JB, Huh YS, Han YK (2015) Highly efficient hydrogen production via water splitting using Pt@MWNT/TiO₂ ternary hybrid composite as a catalyst under UV-visible light. *Synthetic Met* 199: 345-352
14. Kapoor MP, Inagaki S, Yoshida H (2005) Novel zirconium-titanium phosphates mesoporous materials for hydrogen production by photoinduced water splitting. *J Phys Chem B* 109(19):9231-9238

15. Luca V, Blackford MG, Finnie KS, Evans PJ, James M, Lindsay MJ, Skyllas-Kazacos M, Barnes PRF (2007) Sol-gel tungsten oxide/titanium oxide multilayer nanoheterostructured thin films: structural and photoelectrochemical properties. *J Phys Chem C* 111(50):18479–18492
16. Zhou W, Fu HG, Pan K, Tian CG, Qu Y, Lu PP, Sun CC (2008) Mesoporous TiO₂/alpha-Fe₂O₃: bifunctional composites for effective elimination of arsenite contamination through simultaneous photocatalytic oxidation and adsorption. *J Phys Chem C* 112(49):19584–19589
17. Chen KS, Feng XR, Tian H, Li Y, Xie K, Hu R, Cai YX, Gu HS (2014) Silver-decorated titanium dioxide nanotube arrays with improved photocatalytic activity for visible light irradiation. *J Mater Res* 29(11):1302–1308
18. Liu H, He YH, Liang X et al (2014) *J Mater Res* 29(1):98–106
19. Shaislamov U, Yang BL (2013) CdS-sensitized single-crystalline TiO₂ nanorods and polycrystalline nanotubes for solar hydrogen generation. *J Mater Res* 28(3):418–423
20. Guo W, Shen YH, Wu LQ, Gao YR, Ma TL (2011) Effect of N dopant amount on the performance of dye-sensitized solar cells based on N-doped TiO₂ electrodes. *J Phys Chem C* 115(43):21494–21499
21. Xu Z, Yin M, Sun J, Ding G, Lu L, Chang P, Chen X, Li D (2016) 3D periodic multiscale TiO₂ architecture: a platform decorated with graphene quantum dots for enhanced photoelectrochemical water splitting. *Nanotechnology* 27(11):115401
22. Chen L, He S, He BY, Wang TJ, Su CL, Zhang C, Jin Y (2012) Synthesis of iron-doped titanium oxide nanoadsorbent and its adsorption characteristics for fluoride in drinking water. *Ind Eng Chem Res* 51(40):13150–13156
23. Kumaresan L, Mahalakshmi M, Palanichamy M, Murugesan V (2010) Synthesis, characterization, and photocatalytic activity of Sr²⁺ doped TiO₂ nanoplates. *Ind Eng Chem Res* 49(4):1480–1485
24. Zhao DW, Sun XW, Jiang CY, Kyaw AKK, Lo GQ, Kwong DL (2008) Efficient tandem organic solar cells with an Al/MoO₃ intermediate layer. *Appl Phys Lett* 93:8
25. Hamwi S, Meyer J, Winkler T, Riedl T, Kowalsky W (2009) p-type doping efficiency of MoO₃ in organic hole transport materials. *Appl Phys Lett* 94:25
26. Chithambararaj A, Sanjini NS, Velmathi S, Bose AC (2013) Preparation of h-MoO₃ and alpha-MoO₃ nanocrystals: comparative study on photocatalytic degradation of methylene blue under visible light irradiation. *Phys Chem Chem Phys* 15(35):14761–14769
27. Lu MX, Shao CL, Wang KX, Lu N, Zhang X, Zhang P, Zhang MY, Li XH, Liu YC (2014) p-MoO₃ nanostructures/n-TiO₂ nanofiber heterojunctions: controlled fabrication and enhanced photocatalytic properties. *ACS Appl Mater Interfaces* 6(12):9004–9012
28. Zhang XM, Chen YL, Liu RS, Tsai DP (2013) Plasmonic photocatalysis. *Rep Prog Phys* 76:4
29. Yang W, Xiong Y, Zou L, Zou Z, Li D, Mi Q, Wang Y, Yang H (2016) plasmonic Pd nanoparticle-and plasmonic pd nanorod-decorated BiVO₄ electrodes with enhanced photoelectrochemical water splitting efficiency across visible-NIR region. *Nanoscale Res Lett* 11(1):1–8
30. Hou WB, Cronin SB (2013) A review of surface plasmon resonance-enhanced photocatalysis. *Adv Funct Mater* 23(13):1612–1619
31. Hung WH, Lai SN, Su CY, Yin M, Li DD, Xue XZ, Tseng CM (2015) Combined Au-plasmonic nanoparticles with mesoporous carbon material (CMK-3) for photocatalytic water splitting. *Appl Phys Lett* 107:7
32. Ringe E, Sharma B, Henry AI, Marks LD, Van Duyne RP (2013) Single nanoparticle plasmonics. *Phys Chem Chem Phys* 15(12):4110–4129
33. Link S, El-Sayed MA (2000) Shape and size dependence of radiative, non-radiative and photothermal properties of gold nanocrystals. *Int Rev Phys Chem* 19(3):409–453

Submit your manuscript to a SpringerOpen[®] journal and benefit from:

- Convenient online submission
- Rigorous peer review
- Open access: articles freely available online
- High visibility within the field
- Retaining the copyright to your article

Submit your next manuscript at ► springeropen.com
